

Chapter 1

PRECURSORS OF CATASTROPHIC FAILURES

Srutarshi Pradhan¹ and Bikas K. Chakrabarti²

Saha Institute of Nuclear Physics, 1/AF Bidhan Nagar, Kolkata 700064, India

¹*e-mail: spradhan@cmp.saha.ernet.in*

²*e-mail: bikas@cmp.saha.ernet.in*

Abstract We review here briefly the nature of precursors of global failures in three different kinds of many-body dynamical systems. First, we consider the lattice models of self-organised criticality in sandpiles and investigate numerically the effect of pulsed perturbations to the systems prior to reaching their respective critical points. We consider next, the random strength fiber bundle models, under global load sharing approximation, and derive analytically the partial failure response behavior at loading level less than its global failure or critical point. Finally, we consider the two-fractal overlap model of earthquake and analyse numerically the overlap time series data as one fractal moves over the other with uniform velocity. The precursors of global or major failure in all three cases are shown to be very well characterized and prominent.

Keywords: Fracture, earthquake, avalanches in sandpile, self-organised criticality, fiber bundle, fractals, Cantor sets.

1. Introduction

A major failure of a solid or a dynamic catastrophe can often be viewed as a phase transition from an unbroken or non-chaotic phase to a broken or chaotic phase. Some obvious correlations existing in the system before

the failure, are lost in the failure process. However, the equivalence can be made precise and in fact the critical behavior goes to the bone of any failure or catastrophic phenomena.

Several dynamical models of cooperative failure dynamics [1] are now well-studied and their criticality at the global failure point are well established. Here, we have reviewed some of the numerical studies of precursor behavior in two self-organising dynamical [1] models as one approaches the self-organised critical (SOC) point of the avalanches in the lattice sandpile models. The critical behavior of a random fiber bundle model [2] of failure or fracture of a solid under global load sharing is now very precisely demonstrated. The dynamics of failure also become critically slow there and all these have been demonstrated analytically. The precursors of the global failure in the fiber bundle models can therefore be discussed analytically. The resulting universality of the surface roughness in any such fracture process has also been well documented and analysed. The two-fractal overlap model [3] is a very recent modeling approach of earthquake dynamics. The time series of overlap magnitudes obtained, when one fractal slides over the other with uniform velocity, represents the model seismic activity variations. This time series analysis suggests some precursors of large events in this model.

2. Precursors in SOC models of sandpile

A ‘pile’ of dry sand is a unique example SOC system in nature. A growing sandpile gradually comes to a ‘quasi-stable’ state through its self-organising dynamics. This ‘quasi-stable’ state is called the critical state of the system as the system exhibits power law behavior there. Because of avalanches of all sizes, this critical point in the pile is also a catastrophic one. The dynamics of growing sandpiles are successfully modeled by the lattice model [4] of Bak, Tang and Wisenfeld (BTW) in 1987. A stochastic version of sand pile model has been introduced by Manna [5] which also shows SOC, although it belongs to a different universality class. Both the models have been studied extensively at their criticality. Here, we study the sub-critical behavior of both the models and look for the precursors of the critical state.

BTW Model. Let us consider a square lattice of size $L \times L$. At each lattice site (i, j) , there is an integer variable $h_{i,j}$ which represents the height of the sand column at that site. A unit of height (one sand grain) is added at a randomly chosen site at each time step and the system evolves in discrete time. The dynamics starts as soon as any site (i, j) has got a height equal to the threshold value ($h_{th} = 4$): the site topples, i.e., $h_{i,j}$ becomes zero there, and the heights of the four neighboring sites

increase by one unit

$$h_{i,j} \rightarrow h_{i,j} - 4, h_{i\pm 1,j} \rightarrow h_{i\pm 1,j} + 1, h_{i,j\pm 1} \rightarrow h_{i,j\pm 1} + 1. \quad (1.1)$$

If, due to this toppling at site (i, j) , any neighboring site become unstable (its height reaches the threshold value), they in turn follow the same dynamics. The process continues till all sites become stable ($h_{i,j} < h_{th}$ for all (i, j)). When toppling occurs at the boundary of the lattice (four nearest neighbors are not available), extra heights get off the lattice and are removed from the system.

With a very slow but steady rate of addition of unit height (sand grain) at random sites of the lattice, the avalanches get correlated over longer and longer ranges and the average height (h_{av}) of the system grows with time. Gradually the correlation length (ξ) becomes of the order the system size L . Here, on average, the additional height units start leaving the system as the system approaches toward a critical average height $h_c(L)$ and the average height h_{av} remains stable there (see Fig. 1(a)). Also the system becomes critical here (for $L \rightarrow \infty$) as the distributions of the avalanche sizes and the corresponding life times follow robust power laws [4].

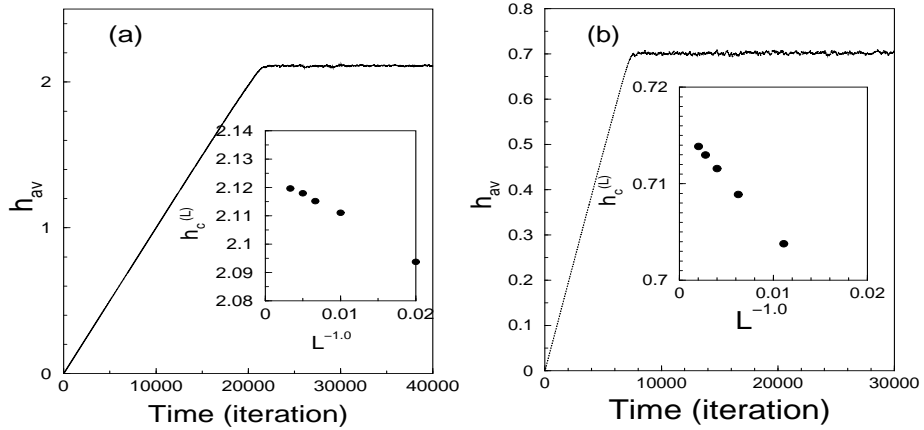


Figure 1. The growth of average height h_{av} against the number of iterations of adding unit heights ($L = 100$). Eventually h_{av} settles at $h_c(L)$. In the inset, we show the finite size behavior of the critical height $h_c(L)$, obtained from simulation results for different L . (a) For the BTW model; (b) for the Manna model.

Here, a finite size scaling fit $h_c(L) = h_c(\infty) + CL^{-1/\nu}$ (obtained by setting $\xi \sim |h_c(L) - h_c(\infty)|^{-\nu} = L$), where C is a constant, with $\nu \simeq$

1.0 gives $h_c \equiv h_c(\infty) \simeq 2.124$ (see inset of Fig. 1(a)). Similar finite size scaling fit with $\nu = 1.0$ gave $h_c(\infty) \simeq 2.124$ in earlier large scale simulations [7].

Manna Model. BTW model is a deterministic one. Manna proposed the stochastic sand-pile model [5] by introducing randomness in the dynamics of sandpile growth. Here, the critical height is 2. Therefore at each toppling the rejected two grains choose their host among the four available neighbors randomly with equal probability. After constant adding of sand grains, the system ultimately settles at a critical state.

We consider now the Manna model on a square lattice of size $L \times L$, where the sites can be either empty or occupied with unit height i.e., the height variables can have binary states $h_{i,j} = 1$ or $h_{i,j} = 0$. A site is chosen randomly and one height is added at that site. If the site is initially empty, it gets occupied:

$$h_{i,j} \rightarrow h_{i,j} + 1, \quad (1.2)$$

If the chosen site is previously occupied then a toppling or ‘hard core interaction’ rejects both the heights from that site:

$$h_{i,j} \rightarrow h_{i,j} - 2, \quad (1.3)$$

and each of these two rejected heights stochastically chooses its host among the 4 neighbors of the toppled site. The toppling can happen in chains if any chosen neighbor was previously occupied and thus cascades are created. After the system attains stable state (dynamics stopped), a new site is chosen randomly and unit height is added to it. Thus the system evolves in discrete time steps. Here again the boundary is assumed to be completely absorbing so that heights can leave the system due to the toppling at the boundary.

With a slow rate of addition of heights (sand grains) at random sites, initially the average height of the system grows with time and soon the system approaches toward a critical average height h_c (see Fig. 1(b)). Here also the critical average height h_c has a finite size dependence and a similar finite size scaling fit $h_c(L) = h_c(\infty) + CL^{-1/\nu}$ gives $\nu \simeq 1.0$ and $h_c \equiv h_c(\infty) \simeq 0.716$ (see inset of Fig. 1(b)). This is close to an earlier estimate $h_c \simeq 0.71695$ [7], made in a somewhat different version of the model. The avalanche size distribution has got power laws similar to the BTW model, at this self-organised critical state at $h_{av} = h_c$. However the exponents seem to be different [5] for this stochastic model, compared to those of BTW model.

Precursors of the SOC point:

In the BTW model. At an average height h_{av} ($< h_c(L)$), when all sites of the system have become stable (dynamics have stopped), a fixed number of height units $h_p = 4$ (pulse of sand grains) is added at any central point of the system. Just after this addition, the local dynamics starts and it takes a finite time or iterations (τ) to return back to the stable state ($h_{i,j} < 4$ for all (i, j)) after several toppling events Δ ; and the disturbance spreads over a length ξ , the correlation length of the system [6, 7]. All these three parameters are seen [7] to diverge as h_{av} approaches the critical height h_c from below following power laws $\tau \sim (h_c - h_{av})^{-\gamma}$, where $\gamma \cong 1.2$; $\Delta \sim (h_c - h_{av})^{-\delta}$, where $\delta \cong 2.0$; $\xi \sim (h_c - h_{av})^{-\nu}$, where $\nu \cong 1.0$ (see Fig. 2).

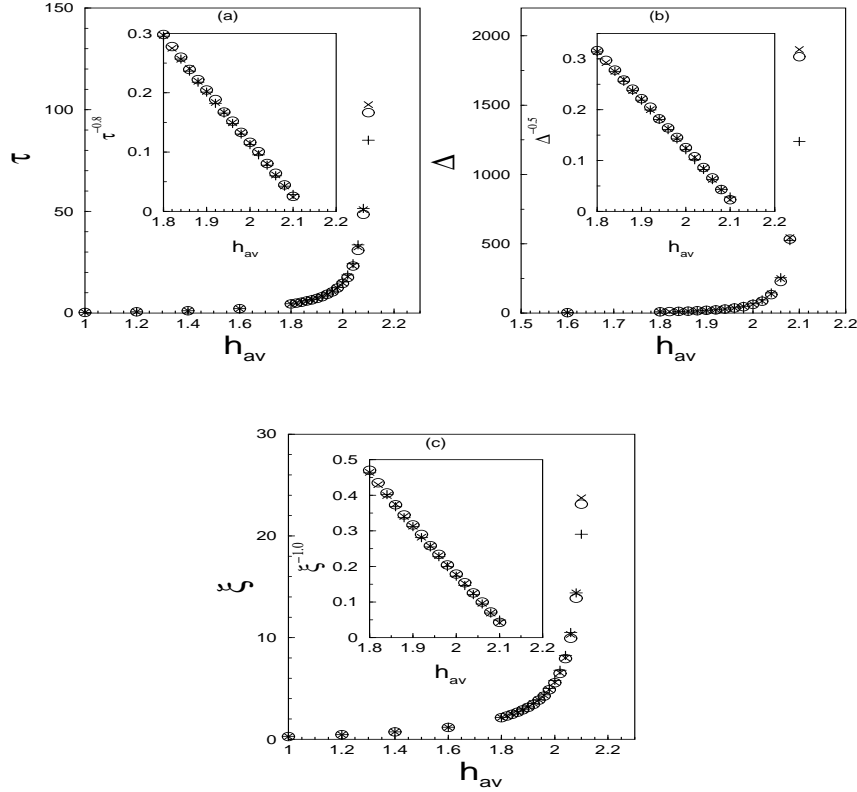


Figure 2. The variations of the precursors with h_{av} ($< h_c(L)$) in the BTW model for different system sizes: $L = 100$ (plus) $L = 200$ (cross) and $L = 300$ (open circle). (a) For relaxation time τ ; in the inset $\tau^{-0.8}$ is plotted against h_{av} . (b) For the total number of topplings Δ ; inset shows $\Delta^{-0.5}$ versus h_{av} plot. (c) For the correlation length ξ ; in the inset, $\xi^{-1.0}$ is plotted against h_{av} .

In the Manna Model. The precursor parameters in Manna model have been measured using similar method as in BTW model. Here the pulse of height is $h_p = 2$ and is added to any arbitrary central site. We get [7] exactly similar power law behaviors for all the parameters as the critical point is approached from below: $\tau \sim (h_c - h_{av})^{-\gamma}$, where $\gamma \cong 1.2$; $\Delta \sim (h_c - h_{av})^{-\delta}$, where $\delta \cong 2.0$; $\xi \sim (h_c - h_{av})^{-\nu}$, where $\nu \cong 1.0$ (see Fig. 3).

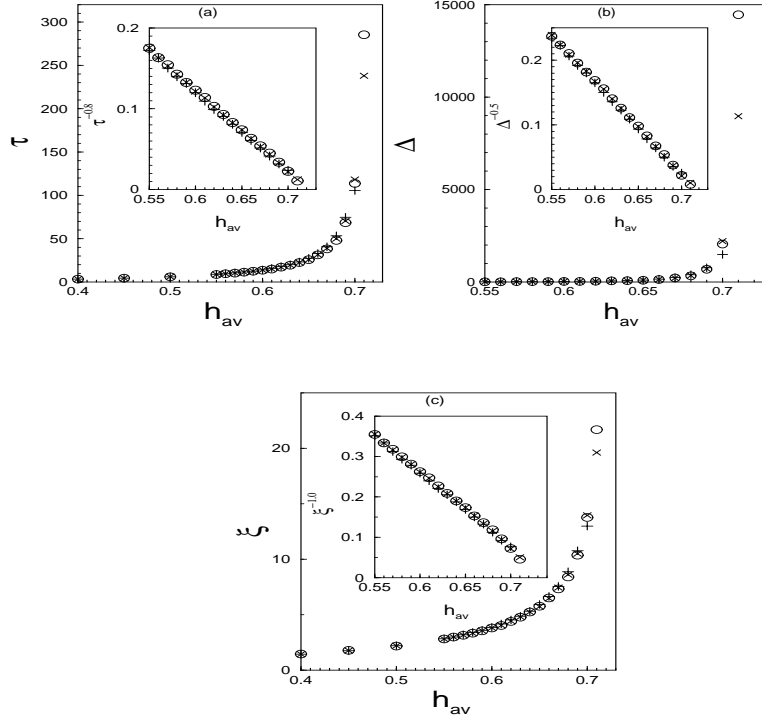


Figure 3. The variations of the precursors with h_{av} ($< h_c(L)$) in the Manna model for different system sizes: $L = 100$ (plus) $L = 200$ (cross) and $L = 300$ (open circle). (a) For relaxation time τ ; in the inset $\tau^{-0.8}$ is plotted against h_{av} . (b) For the total number of topplings Δ ; inset shows $\Delta^{-0.5}$ versus h_{av} plot. (c) For the correlation length ξ ; in the inset, $\xi^{-1.0}$ is plotted against h_{av} .

The Monte Carlo studies showed that these response parameters like the relaxation time τ , size of the damage Δ and its radial size ξ , all tend to diverge, following the above mentioned robust power laws, in both the models. Precise knowledge of these power laws can therefore help estimating the critical or catastrophic point (h_c) by extrapolating the inverse power of these quantities for informations at h_{av} ($< h_c$) (see insets of Figs. 2 and 3). Similar critical slowing down phenomena should be of interest in the context of magnetohydrodynamics of plasma [8].

3. Precursors of fracture-failure in fiber bundles

The fiber bundle model was introduced by Peirce [2] in the context of testing the strength of cotton yarns. Fiber bundles are of two classes with respect to the time dependence of fiber strength: The ‘static’ bundles contain fibers whose strengths are independent of time, where as the ‘dynamic’ bundles are assumed to have time dependent elements to capture the creep rupture and fatigue behaviors. According to the load sharing rule, fiber bundles are being classified into two groups: Global load-sharing (democratic) bundles and local load-sharing bundles. In democratic bundles intact fibers bear the applied load equally and in local load-sharing bundles the terminal load of the failed fiber is given equally to all the intact neighbors. With steadily increasing load, the fiber bundles approach their respective failure point obeying a dynamics determined by the load sharing rule. The phase transition [9] and dynamic critical behavior of the fracture process in such democratic bundles has been established through recursive formulation [2, 9] of the failure dynamics. The exact solutions of the recursion relations in the global load-sharing case suggest universal values of the exponents involved.

We discuss here the failure of a static fiber bundles under global load sharing (democratic bundles) with steadily increasing load on the bundles. We show analytically the variation of associated precursor parameters with the applied stress which help to estimate the failure point accurately.

The model assumes equal load sharing, i.e., the intact fibers share the applied load equally. The strength of each of the fibers in the bundle is determined by the stress value (σ_{th}) it can bear, and beyond which it fails. The strength of the fibers are taken from a randomly distributed normalised density $\rho(\sigma_{th})$ within the interval 0 and 1 such that

$$\int_0^1 \rho(\sigma_{th}) d\sigma_{th} = 1. \quad (1.4)$$

The global load sharing assumption neglects ‘local’ fluctuations in stress (and its redistribution) and renders the model as a mean-field one.

Breaking dynamics of the democratic bundles. The breaking dynamics starts when an initial stress σ (load per fiber) is applied on the bundle. The fibers having strength less than σ fail instantly. Due to this rupture, total number of intact fibers decreases and now these intact fibers have to bear the applied load on the bundle. Hence effective stress on the fibers increases and this compels some more fibers to break.

These two sequential operations, the stress redistribution and further breaking of fibers continue till an equilibrium is reached, where either the surviving fibers are strong enough to bear the applied load on the bundle or all fibers fail.

This breaking dynamics can be represented by recursion relations in discrete time steps. Let U_t be the fraction of fibers in the initial bundle that survive after time step t , where time step indicates the number of (elemental) stress redistributions. Then the redistributed load per fiber after t time step becomes

$$\sigma_t = \frac{\sigma}{U_t}; \quad (1.5)$$

and after $t + 1$ time steps the surviving fraction of fiber is

$$U_{t+1} = 1 - P(\sigma_t); \quad (1.6)$$

where $P(\sigma_t)$ is the cumulative probability of corresponding density distribution $\rho(\sigma_{th})$:

$$P(\sigma_t) = \int_0^{\sigma_t} \rho(\sigma_{th}) d\sigma_{th}. \quad (1.7)$$

Using now Eqns. (1.5) and (1.6) we can write the recursion relations which show how σ_t and U_t evolve in discrete time:

$$\sigma_{t+1} = \frac{\sigma}{1 - P(\sigma_t)}; \sigma_0 = \sigma \quad (1.8)$$

and

$$U_{t+1} = 1 - P(\sigma/U_t); U_0 = 1. \quad (1.9)$$

The recursion relations (1.5) and (1.6) represent the basic dynamics of failure in global load sharing models. At the equilibrium or steady state $U_{t+1} = U_t \equiv U^*$ and $\sigma_{t+1} = \sigma_t \equiv \sigma^*$. This corresponds to a fixed point of the recursive dynamics. Eqn. (1.6) can be solved at the fixed point for some particular distribution of $\rho(\sigma_{th})$ and these solutions near U^* (or σ^*) give the detail features of the failure dynamics of the bundle.

Precursors of global failure:

For uniform distribution of fiber strength. We choose first the uniform density of fiber strength distribution to solve the recursive failure dynamics of democratic bundle. Here, the cumulative probability becomes

$$P(\sigma_t) = \int_0^{\sigma_t} \rho(\sigma_{th}) d\sigma_{th} = \int_0^{\sigma_t} d\sigma_{th} = \sigma_t. \quad (1.10)$$

Therefore U_t follows a simple recursion relation (following Eqn. (1.6))

$$U_{t+1} = 1 - \frac{\sigma}{U_t}. \quad (1.11)$$

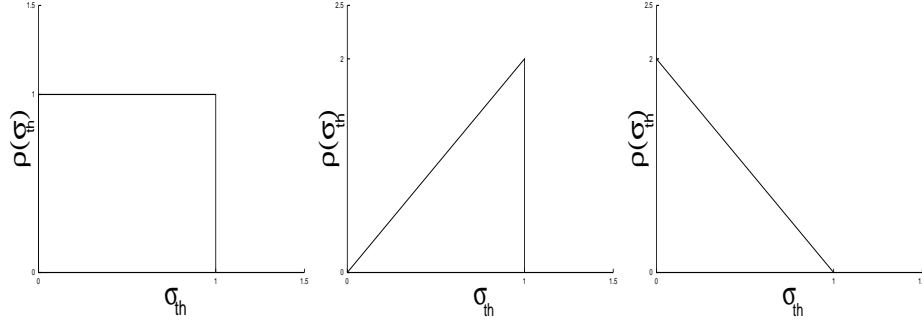


Figure 4. Three simple models considered here assume (a) uniform, (b) linearly increasing and (c) linearly decreasing density $\rho(\sigma_{th})$ of the fiber strength distribution up to a cutoff strength.

At the equilibrium state ($U_{t+1} = U_t = U^*$), the above relation takes a quadratic form of U^* :

$$U^{*2} - U^* + \sigma = 0. \quad (1.12)$$

The solution is

$$U^*(\sigma) = \frac{1}{2} \pm (\sigma_c - \sigma)^{1/2}; \sigma_c = \frac{1}{4}. \quad (1.13)$$

Here σ_c is the critical value of the initial applied stress beyond which the bundle fails completely. The solution with (+) sign is the stable one, whereas the one with (-) sign gives unstable solution. The quantity $U^*(\sigma)$ must be real valued as it has a physical meaning: it is the fraction of the original bundle that remains intact under a fixed applied stress σ when the applied stress lies in the range $0 \leq \sigma \leq \sigma_c$. Clearly, $U^*(\sigma_c) = 1/2$ (putting $\sigma = \sigma_c$ in Eqn. (1.13)). Therefore the stable solution can be written as

$$U^*(\sigma) = U^*(\sigma_c) + (\sigma_c - \sigma)^{1/2}; \sigma_c = \frac{1}{4}. \quad (1.14)$$

For $\sigma > \sigma_c$ we can not get a real-valued fixed point as the dynamics never stops until $U_t = 0$, when the bundle breaks completely. It may be noted that the quantity $U^*(\sigma) - U^*(\sigma_c)$ behaves like an order parameter that determines a transition from a state of partial failure ($\sigma \leq \sigma_c$) to a state of total failure ($\sigma > \sigma_c$) [9]:

$$O \equiv U^*(\sigma) - U^*(\sigma_c) = (\sigma_c - \sigma)^\beta; \beta = \frac{1}{2}. \quad (1.15)$$

To study the dynamics away from criticality ($\sigma \rightarrow \sigma_c$ from below), we replace the recursion relation (1.11) by a differential equation

$$-\frac{dU}{dt} = \frac{U^2 - U + \sigma}{U}. \quad (1.16)$$

Close to the fixed point we write $U_t(\sigma) = U^*(\sigma) + \epsilon$ (where $\epsilon \rightarrow 0$). This, following Eq. (1.13), gives [9]

$$\epsilon = U_t(\sigma) - U^*(\sigma) \approx \exp(-t/\tau), \quad (1.17)$$

where $\tau = \frac{1}{2} \left[\frac{1}{2}(\sigma_c - \sigma)^{-1/2} + 1 \right]$. Near the critical point we can write

$$\tau \propto (\sigma_c - \sigma)^{-\alpha}; \alpha = \frac{1}{2}. \quad (1.18)$$

Therefore the relaxation time diverges following a power-law as $\sigma \rightarrow \sigma_c$ from below [9].

One can also consider the breakdown susceptibility χ , defined as the change of $U^*(\sigma)$ due to an infinitesimal increment of the applied stress σ [7, 9]

$$\chi = \left| \frac{dU^*(\sigma)}{d\sigma} \right| = \frac{1}{2}(\sigma_c - \sigma)^{-\eta}; \eta = \frac{1}{2} \quad (1.19)$$

from Eqn. (1.13). Hence the susceptibility diverges as the applied stress σ approaches the critical value $\sigma_c = \frac{1}{4}$. Such a divergence in χ had already been observed in the numerical studies [7].

For linearly increasing distribution of fiber strength. Here, the cumulative probability becomes

$$P(\sigma_t) = \int_0^{\sigma_t} \rho(\sigma_{th}) d\sigma_{th} = 2 \int_0^{\sigma_t} \sigma_{th} d\sigma_{th} = \sigma_t^2. \quad (1.20)$$

Therefore U_t follows a recursion relation (following Eq. (1.6))

$$U_{t+1} = 1 - \left(\frac{\sigma}{U_t} \right)^2. \quad (1.21)$$

At the fixed point ($U_{t+1} = U_t = U^*$), the above recursion relation can be represented by a cubic equation of U^*

$$(U^*)^3 - (U^*)^2 + \sigma^2 = 0. \quad (1.22)$$

Solving the above equation we get [9] the value of critical stress $\sigma_c = \sqrt{4/27}$ which is the strength of the bundle for the above fiber strength distribution. Here, the order parameter, susceptibility, relaxation time all follow the same power laws (Eqns. (1.15), (1.18) and (1.19)) observed for uniform strength distribution.

For linearly decreasing distribution of fiber strength. In this case, the cumulative probability becomes

$$P(\sigma_t) = \int_0^{\sigma_t} \rho(\sigma_{th}) d\sigma_{th} = 2 \int_0^{\sigma_t} (1 - \sigma_{th}) d\sigma_{th} = 2\sigma_t - \sigma_t^2 \quad (1.23)$$

and U_t follows a recursion relation (following Eqn. (1.6))

$$U_{t+1} = 1 - 2\frac{\sigma}{U_t} + \left(\frac{\sigma}{U_t}\right)^2. \quad (1.24)$$

At the fixed point ($U_{t+1} = U_t = U^*$), the above recursion relation can be represented by a cubic equation of U^*

$$(U^*)^3 - (U^*)^2 + 2\sigma U^* - \sigma^2 = 0. \quad (1.25)$$

Solution of the above equation gives [9] the value of critical stress $\sigma_c = 4/27$ which is the strength of the bundle. Here also, the precursor parameters, the order parameter, susceptibility and relaxation time, all follow the same power laws (Eqns. (1.15), (1.18) and (1.19)) observed for uniform strength distribution.

Thus the democratic fiber bundles (for different fiber strength distributions) show phase transition from a state of partial failure to total failure with a well defined precursors (order parameter, susceptibility and relaxation time) which show similar power law variation on the way as the critical point is approached; characterized by the universal values of the associated exponents (α , β and η). All the above scaling behaviors represented by Eqns. (1.15), (1.18) and (1.19) for stress (σ) below the global failure stress (σ_c) of the bundle suggests that a prior knowledge of the responses like the fraction of failed fibers, relaxation time etc. can be extrapolated following the above power laws to estimate the global failure point σ_c .

4. Two-fractal overlap model of earthquake and the prediction possibility of large events

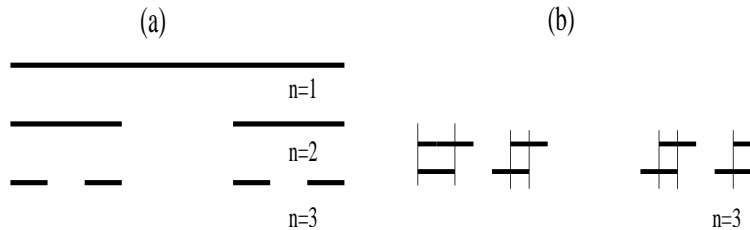
The two-fractal overlap model of earthquake [3] is a very recent modeling attempt. Such models are all based on the observed ‘plate tectonics’

and the fractal nature of the interface between tectonic plates and earth's solid crust. The statistics of overlaps between two fractals is not studied much yet, though their knowledge is often required in various physical contexts. For example, it has been established recently that since the fractured surfaces have got well-characterized self-affine properties [10], the distribution of the elastic energies released during the slips between two fractal surfaces (earthquake events) may follow the overlap distribution of two self-similar fractal surfaces [3, 11]. Chakrabarti and Stinchcombe [3] had shown analytically that for regular fractal overlap (Cantor sets and carpets) the contact area distribution follows a simple power law decay. The two fractal overlap magnitude changes in time as one fractal moves over the other. The overlap (magnitude) time series can therefore be studied as a model time series of earthquake avalanche dynamics [12].

Here, we study the time (t) variation of contact area (overlap) $m(t)$ between two well-characterized fractals having the same fractal dimension as one fractal moves over the other with constant velocity. We have chosen only very simple fractals: regular and random Cantor sets, gaskets and percolating cluster. We analyse the time series data of Cantor set overlaps only to find the prediction possibility of large events (occurrence of large overlaps). We show that the time series $m(t)$ obtained by moving one fractal uniformly over the other (with periodic boundary condition) has some features which can be utilized to predict the 'large events'. This is shown utilizing the discrete or a 'quantum' nature of the integrated (cumulative) overlap over time.

Two-fractal overlaps:

We now discuss the two-fractal overlap sizes. Let us take two identical Cantor sets at finite generation and slide one over the other, assuming periodic boundary condition. Two such cases for a regular Cantor sets as well as a gasket are shown in Fig. 5. Similar cases for random fractals are shown in Fig. 6.



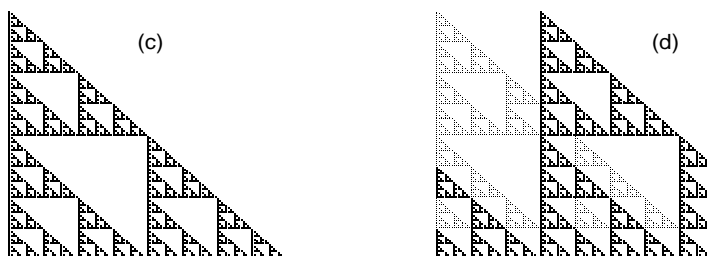


Figure 5. (a) A regular Cantor set of dimension $\ln 2 / \ln 3$; only three finite generations are shown. (b) The overlap of two identical (regular) Cantor sets, at $n = 3$, when one slips over the other; the overlap sets are indicated within the vertical lines, where periodic boundary condition has been used. (c) A regular gasket of dimension $\ln 3 / \ln 2$ at the 7th generation. (d) The overlap of two identical regular gaskets at same generations ($n = 7$) is shown as one is translated over the other; periodic boundary condition has been used for the translated gasket.

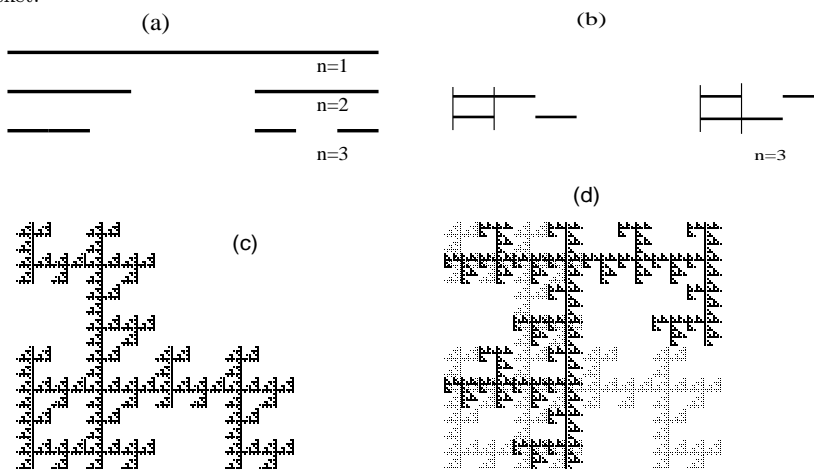


Figure 6. (a) A random Cantor set of dimension $\ln 2 / \ln 3$; only three finite generations are shown. (b) Overlap of two random Cantor sets (at $n = 3$; having the same fractal dimension) in two different realisations. The overlap sets are indicated within the vertical bars. (c) A random realisation of a gasket of dimension $\ln 3 / \ln 2$ at 7th generation. (d) The overlap of two random gaskets of same dimension and of same generation but generated in different realisations.

Next, we study the overlap distribution of two well-characterised random fractals; namely the percolating fractals [13]. It seems, although many detailed features of the clusters will change with the changes in (parent) fractals, the subtle features of the overlap distribution function remains unchanged.

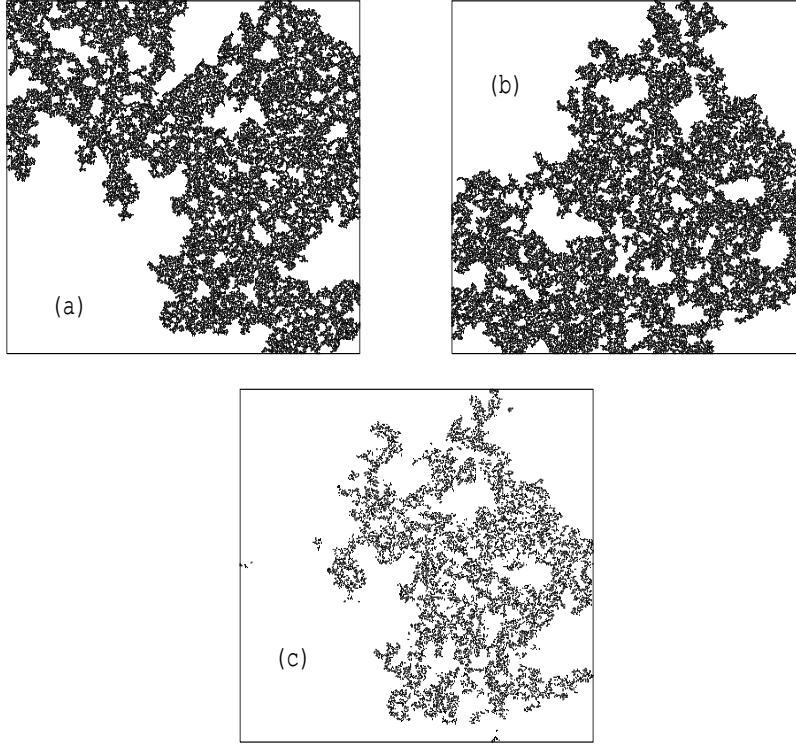


Figure 7. The overlap between two percolating clusters; (a) and (b) are two typical realisations of the same percolating fractal on square lattice ($d_f \simeq 1.89$) and (c) their overlap set. Note, the overlap set need not be a connected one.

Our earlier study [9] on the overlap statistics for regular and random Cantor sets, gaskets and percolating clusters indicated a universal scaling behavior of the overlap or contact area (m) distributions $P(m)$ for all types of fractal set overlaps mentioned: $P'(m') = L^\alpha P(m, L)$; $m' = mL^{-\alpha}$, where L denotes the finite size of the fractal and the exponent $\alpha = 2(d_f - d)$; d_f being the mass dimension of the fractal and d is the embedding dimension. Also the overlap distribution $P(m)$, and hence the scaled distribution $P'(m')$, are seen to decay with m or m' following a power law (with exponent value equal to the embedding dimension of the fractals) for both regular and random Cantor sets and gaskets: $P(m) \sim m^{-\beta}$; $\beta = d$. However, for the percolating clusters [13], the overlap size distribution takes a Gaussian form.

We consider now the time series obtained by counting the overlaps $m(t)$ as a function of time as one Cantor set moves over the other (periodic boundary condition is assumed) with uniform velocity. The analysis presented here follows our previous study [14].

Overlap time series data. The time series are shown in Fig. 8, for finite generations of Cantor sets of dimensions $\ln 2/\ln 3$ and $\ln 4/\ln 5$ respectively.

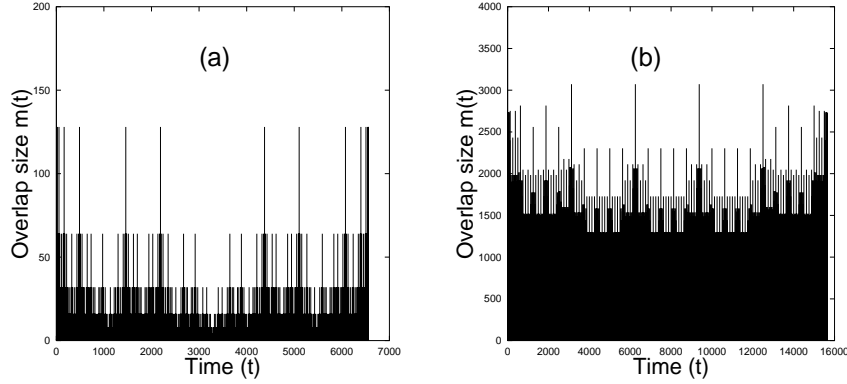


Figure 8. The time (t) series data of overlap size (m) for regular Cantor sets: (a) of dimension $\ln 2/\ln 3$, at 8th generation; (b) of dimension $\ln 4/\ln 5$, at 6th generation. The obvious periodic repeat of the time series comes from the assumed periodic boundary condition of one of the sets (over which the other one slides).

Cumulative overlap sizes. Now we calculate the cumulative overlap size $Q(t) = \int_0^t m dt$ and plot that against time in Fig. 9. Note, that ‘on average’ $Q(t)$ is seen to grow linearly with time t for regular as well as random Cantor sets. This gives a clue that instead of looking at the individual overlaps $m(t)$ series one may look for the cumulative quantity. We observe $Q(t) \simeq ct$, where c is dependent on the fractal. This result is even more prominent in the case of Cantor sets with $d_f = \ln 4/\ln 5$.

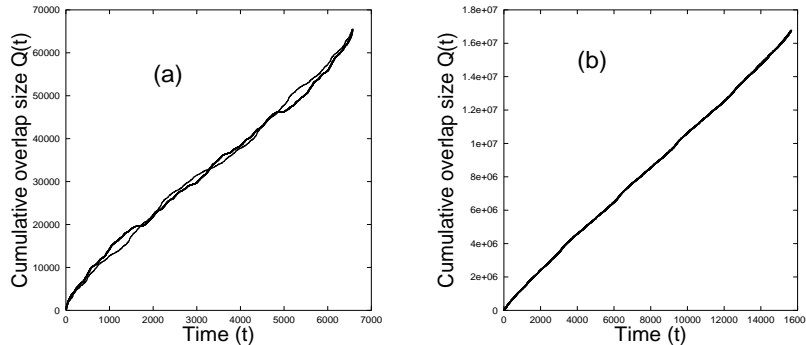


Figure 9. The cumulative overlap Q versus time; for pure Cantor sets: (a) of dimension $\ln 2/\ln 3$ (at 8th generation) and (b) of dimension $\ln 4/\ln 5$ (at 6th generation). The dotted line corresponds to those for two identical but random Cantor sets. In (b) the two lines fall on each other.

Cumulative overlap quantization. We first identify the ‘large events’ occurring at time t_i in the $m(t)$ series, where $m(t_i) \geq M$, a pre-assigned magnitude. We then look for the cumulative overlap size $Q_i(t) = \int_{t_{i-1}}^t m dt$, $t \leq t_i$, where the successive large events occur at times t_{i-1} and t_i . The behavior of Q_i with time is shown in Fig. 10 for regular cantor sets with $d_f = \ln 2/\ln 3$ at generation $n = 8$. Similar results are also given for Cantor sets with $d_f = \ln 4/\ln 5$ at generation $n = 6$ in Fig. 11. $Q_i(t)$ is seen to grow almost linearly in time up to $Q_i(t_i)$ after which it drops down to zero. It appears that there are discrete (quantum) values of $Q_i(t_i)$. One can therefore anticipate large events when the cumulative seismic overlap $Q_i(t)$, since the last major event at t_{i-1} , grows linearly with time t to the discrete levels lQ_0 , specific to the series of events. No major event occurs during the growth period of $Q_i(t)$ for the intermediate values.

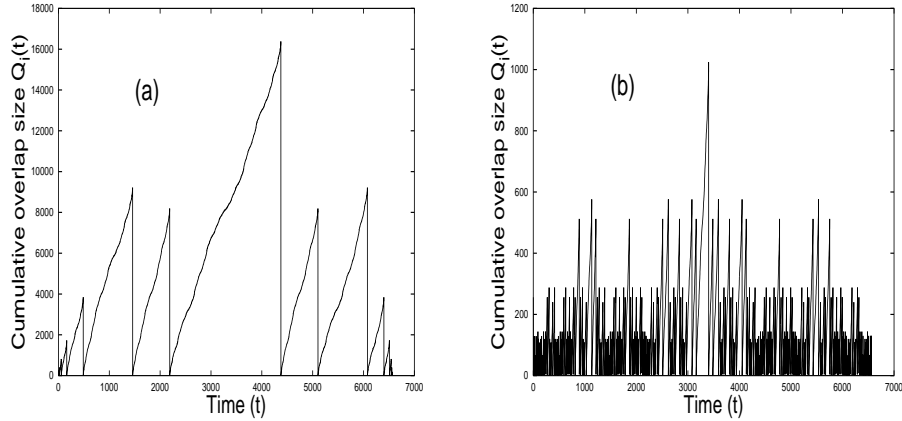


Figure 10. The cumulative overlap size variation with time (for regular Cantor sets of dimension $\ln 2/\ln 3$, at 8th generation), where the cumulative overlap has been reset to 0 value after every big event (of overlap size $\geq M$ where $M = 128$ (a) and 32 (b) respectively).

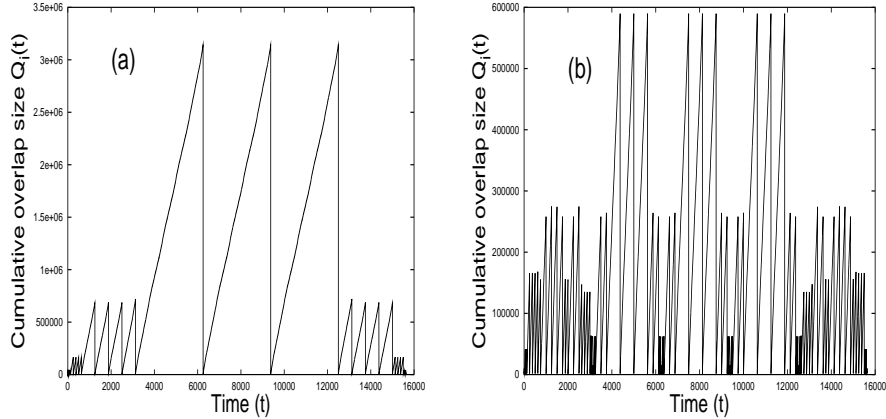


Figure 11. The cumulative overlap size variation with time (for regular Cantor sets of dimension $\ln 4 / \ln 5$, at 6th generation), where the cumulative overlap has been reset to 0 value after every big event (of overlap size $\geq M$ where $M = 2400$ (a) and 2048 (b) respectively).

5. Summary and Discussions

In all the dynamical models of sandpile avalanches (discussed in section 2), we find that the growing correlations in the dynamics of constituent elements manifest themselves as various precursors. The number of topplings Δ , relaxation time τ and the correlation length ξ , in both BTW and Manna model, grow and diverge following power laws as the systems approach their respective critical points h_c from below (see Figs. 2 and 3): $\Delta \sim (h_c - h_{av})^{-\delta}$, $\tau \sim (h_c - h_{av})^{-\gamma}$ and $\xi \sim (h_c - h_{av})^{-\nu}$. For two dimensional systems, we find numerically here $\delta \simeq 2.0$, $\gamma \simeq 1.2$ and $\nu \simeq 1.0$ for both BTW and Manna model. Basically, we studied the behavior for $h_{av} < h_c$, the precursor behavior, where ξ is necessarily finite. As we add here the tiny pulse at some central site of a relatively large system, the boundary effect can not be really felt because of the smallness of ξ compared to L for most values of h_{av} . This explains the lack of finite size effect in our precursor studies.

For the global failure or fracture in fiber bundle models (discussed in section 3), we find that the breakdown susceptibility χ (giving the increment in the number of broken fibers for an infinitesimal increment of load on the bundle) and the corresponding relaxation time τ (required for the bundle to stabilise, after successive failures of the fibers), both diverge as the external load or stress approaches its global failure point σ_c from below: $\tau \sim (\sigma_c - \sigma_{av})^{-\alpha}$ and $\chi \sim (\sigma_c - \sigma_{av})^{-\eta}$; $\alpha = \eta = 1/2$. These results are of course analytically derived for different fiber strength distributions and the universality class of the model has been confirmed.

If one Cantor set moves uniformly over another, the overlap between the two fractals change quasi-randomly with time (see eg., Fig. 8). These time series are taken as model seismic activity variations in such two-fractal overlap model of earthquake. The overlap size distribution was argued [3] and shown [9] to follow power law decay. We showed numerically (see section 4) that if one fixes a magnitude M of the overlap sizes m , so that overlaps with $m \geq M$ are called ‘events’ (or earthquake), then the cumulative overlap $Q_i(t) = \int_{t_{i-1}}^t m dt$, $t \leq t_i$, (where two successive events of $m \geq M$ occur at times t_{i-1} and t_i) grows linearly with time up to some discrete quanta $Q_i(t_i) \cong lQ_0$, where Q_0 is the minimal overlap quantum, dependent on M and n (the generation number). Here l is an integer (see Figs. 10, 11) [14]. Although our results here are for regular fractals of finite generation n , the observed discretisation of the overlap cumulant Q_i with the time limit set by n , is a robust feature and can be seen for larger time series for larger generation number n . This part of the model study therefore indicates that one can note the growth of the cumulant seismic response $Q_i(t)$, rather than the seismic event strength $m(t)$, and anticipate some big events as the response reaches the discrete levels lQ_0 , specific to the series of events.

Some prior knowledge of the precursors and their precise behavior (power laws etc.), as discussed here for three different kinds of failure models of cooperatively interacting dynamical systems which are prone to major failures, are therefore plausible. These precursor responses should help estimating the location of the global failure or critical point using proper extrapolation of the above quantities, which are available long before the failure occurs. The usefulness of such precursors can hardly be overemphasized.

Acknowledgments

We are grateful to our collaborators P. Bhattacharyya, P. Choudhuri and P. Ray for useful discussions.

References

- [1] B. K. Chakrabarti and L. G. Benguigui, *Statistical Physics of Fracture and Breakdown in Disorder Systems*, Oxford Univ. Press, Oxford (1997); H. J. Herrmann and S. Roux (Eds), *Statistical Models for the Fracture of Disordered Media*, North Holland, Amsterdam (1990); P. Bak, *How Nature Works*, Oxford Univ. Press, Oxford (1997).
- [2] F. T. Peires, *J. Textile Inst.* **17**, T355 (1926); H. E. Daniels, *Proc. R. Soc. London A* **183** 405 (1945); S. L. Phoenix and R. L. Smith, *Int.*

- J. Solid Struct. **19**, 479 (1983); R. da Silveira, Am. J. Phys. **67** 1177 (1999); E. Altus, Mech. Mater. **34** 257 (2002); S. Pradhan and B. K. Chakrabarti, Proc. DMTAS (Chennai, March 2003), Int. J. Mod. Phys. B (in press), cond-mat/0307734.
- [3] B. K. Chakrabarti, R. B. Stinchcombe, Physica A, **270** 27 (1999).
- [4] P. Bak, C. Tang and K. Wiesenfeld, Phys. Rev. Lett. **59** 381 (1987); D, Dhar, Phys. Rev. Lett. **64** 1613 (1990).
- [5] S. S. Manna, J. Phys. A: Math. Gen. **24** L363 (1991); D. Dhar, Physica A **270** 69 (1999).
- [6] M. Acharyya and B. K. Chakrabarti, Physica A **224** 254 (1996); Phys. Rev. E **53** 140 (1996).
- [7] S. Pradhan and B. K. Chakrabarti, Phys. Rev. E **65**, 016113 (2001).
- [8] S. Ortolani and D. D. Schnack, *Magnetohydrodynamics of Plasma Relaxation*, World Scientific Publ., Singapore (1993).
- [9] S. Pradhan, P. Bhattacharyya and B. K. Chakrabarti, Phys. Rev. E **66**, 016116 (2002); P. Bhattacharyya, S. Pradhan and B. K. Chakrabarti, Phys. Rev. E **67**, 046122 (2003).
- [10] B. B. Mandelbrot, *The Fractal Geometry of Nature* Freeman, San Francisco (1982); B. B. Mandelbrot, D. E. Passoja, A. J. Pullay, Nature **308** 721 (1984); A. Hansen and J. Schmittbuhl, Phys. Rev. Lett. **90**, 045504 (2003); J. O. H. Bakke, J. Bjelland, T. Ramstad, T. Strandén, A. Hansen and J. Schmittbuhl, Proc. UASP03 (Kolkata, March 2003), Physica Scripta **T106** 65 (2003).
- [11] S. Pradhan, B. K. Chakrabarti, P. Ray and M. K. Dey, Proc. UASP03 (Kolkata, March 2003), Physica Scripta **T106** 77 (2003).
- [12] J. M. Carlson, J. S. Langer and Shaw, Rev. Mod. Phys. **62** 2632 (1989).
- [13] See e.g., D. Stauffer and A. Aharony, *Introduction to Percolation Theory*, Taylor and Francis, London (1994).
- [14] S. Pradhan, P. Choudhuri and B. K. Chakrabarti, in *Proc. NATO conf. (CMD-10, Soresh, Israel, July 2003)*, *Continuum Models of Discrete Systems*, Eds. D. J. Bergman and E. Inan, Kluwer Acad. Pub., New York, cond-mat/0307735.